

Computational Studies of PVDF and P(VDF-TrFE) Nanofilms Polarization During Phase Transition Revealed by Emission Spectroscopy

Bystrov V.S.^{*1,2}, Paramonova E.V.¹, Dekhtyar Y.³, Katashev A.³, Polyaka N.³, Bystrova A.V.⁴, Sapronova A.V.⁵, Fridkin V.M.⁶, Kliem H.⁷, Kholkin A.L.²

¹*Institute of Mathematical Problems of Biology RAS, Pushchino, Russia*

²*Department of Ceramics and Glass Engineering & CICECO, University of Aveiro, Aveiro, Portugal*

³*Institute of Biomedical Engineering and Nanotechnology, Riga Technical University, Riga, Latvia*

⁴*Institute of Theoretical and Experimental Biophysics RAS, Pushchino, Russia*

⁵*Bergen Centre for Computational Science, Unifob AS, Bergen, Norway*

⁶*Institute of Crystallography, RAS, Moscow, Russia*

⁷*Institute of Electrical Engineering Physics, University of Saarland, Saarbruecken, Germany*

Abstract. Electronic structure and self-polarization of P(VDF-TrFE) Langmuir-Blodgett nanofilms according to their thickness, composition and structural conformation under temperature phase transition were analyzed. Both thermo-stimulated exoelectron emission (TSEE) spectroscopy and computational simulation, including quantum-chemical calculations from first principles, were provided. PVDF and composite P(VDF-TrFE) (70:30) molecular chains as Trans and Gauche conformers as well as crystal cells were modeled for these agreed-upon TSEE analyses. The quantum-chemical calculations and the computational simulation were based on the density functional theory (DFT) as well as semi-empirical (PM3) methods. It was demonstrated that the energies of electron states as well as the total energies of the studied PVDF and P(VDF-TrFE) molecular clusters during phase transformation influenced electron work function and electron affinity. The performed combined analysis of the TSEE experimental data as well as the computational data of the molecular models showed the effectiveness of that joined approach. TSEE for the first time was in use for contactless measurements of nanofilm polarization and characterizations of the phase transition. The proposed new method can be widely used in nanobiomedicine, particularly in development of new bone bio-implants, including built-in sensors (new smart nanotechnology).

Key words: *polymer ferroelectrics, polarization and depolarization, thermo-stimulated exoelectron emission, computational molecular modeling, density functional theory, semi-empirical method, electron band energies, electron work function and affinity.*

INTRODUCTION

Ferroelectric thin Langmuir–Blodgett (LB) films, based on the poly(vinylidene fluoride) (PVDF) and poly(vinylidene fluoride–trifluoroethylene) P(VDF–TrFE) copolymers, clearly demonstrated polarization switching phenomena on nanometer size scale with local ferroelectric polarization reversal on the atomic-molecular level [1–5]. Now these LB polymer films are widely explored, using of various techniques, including nanoscale characterization by piezoresponse force microscopy (PFM) method [6–11], as novel prospective ferroelectric nano-material for their applications in nanotechnology and microelectronics, for data storage and new non-volatile memory cells [12], in biomedicine and nanomedicine as a promising component of various nanocomposites due to their acoustic and piezoelectric properties having a high compatibility with many organic and biological molecules and tissues [13–18]. Nevertheless many of these important physical and structural properties of the PVDF copolymers thin films are not clear yet. Especially it refers to its polarization switching phenomena in various conditions and compositions. One of promising ideas is to use actuators made of biocompatible polyvinylidene fluoride (PVDF) piezoelectric materials. An actuator is placed on an implant's surface and stimulates bone growth by electrical and mechanical stimulation of osteoblast cells [19, 20] due to high surface charge – polarization of PVDF and P(VDF–TrFE). As such, they are similar to recently developed highly polarized (surface charged) hydroxyapatite (HAP) [21], especially in the form of nanostructured porous ceramics (PERCERAMICS) [22]. It has been showed that the number of attached osteoblasts sharply increases on the negatively charged HAP surface [23].

As it is well known, in ferroelectrics polarization is coupled with piezoelectric constants [24]. Use of PVDF means that mechanical stimulation of bone growth depends on the amount of electrical energy applied only, and that the bone growth can be stimulated in different directions by changing piezoelectric constants. This concept of smart structures can be adapted to other active devices. In this case it is necessary to know mechanisms of charging (polarization formation) and be able to control them. It is important not to distort the dynamics of the behaviour of the controlled object.

Such non-contact measurements of the surface charge (polarization) can be performed by the method of thermo-stimulated exoelectronic emission (TSEE) [25–27], which allows us of measuring of changes in work function, and determining the value of surface charge (polarization). For correct determination of the polarization it is necessary to have a corresponding correct molecular model for the mechanisms of the processes occurring in the surface layers of the sample. For this purpose, computational modeling from first principles and studies for several structures of the PVDF and P (VDF–TrFE) molecular models at different phase conformations – Trans (T) and Gauche (G) – have been performed. The appropriate structures of the two states of the sample – in a polar ferroelectric phase and a nonpolar paraelectric phase – were determined, corresponding to the molecular models of P(VDF–TrFE) crystal cells in the Trans and Gauche conformations. The obtained data allowed us of calculating of electronic spectra and constructing of diagrams of energy bands for these two different phases, as well as determining of the gap (forbidden energy band) and its changes during phase transition. It is important that these parameters depend on the internal electric field that determines their tilting and the shift, which appears on the surface, as a function of surface charge (polarization). On the other hand, changes of the surface charge alter the work function measured by TSEE: in different phases (and conformations) these changes vary. The created model, based on the energy band structures and their changes during phase transition, allows us of non-contact measuring of polarization through the data of the work function, registered by TSEE.

In this paper we report on our studies of polarization properties of PVDF copolymer films by the use, for the first time for these purposes, of a novel contactless method - thermo-stimulated exoelectron emission (TSEE) analysis [25–27], coupled with molecular modeling from first principles. These studies continue the series of our previous investigations of ferroelectric and nanoscale properties of thin LB PVDF copolymer films [11, 16–18]. The proposed new method can be widely used in bionanomedicine, particularly in the development of new bone bio-implants, including built-in sensors (new smart nanotechnology).

EXPERIMENTAL AND COMPUTATIONAL DETAILS

1. Preparation of samples

Preparation, structure, phase transitions and ferroelectric properties of poly(vinylidene fluoride-trifluoroethylene) P(VDF–TrFE) films prepared by Langmuir–Blodgett (LB) method were described in detail in [1–3]. They manifested spontaneous polarization $P_s \sim 0.1 \text{ cm}^{-2}$ in the polar orthorhombic phase “2mm” (according to the standard crystallographic classification). At 80–100 °C (depending on the proportion of VDF to TrFE) the copolymer passes into the nonpolar hexagonal phase “6:m” via a first-order phase transition. High-quality thin films of ferroelectric P(VDF–TrFE), (70:30) were produced by the LB method using the horizontal Schafer variation of the LB technique. The optimal surface pressure on the isotherm was chosen $6 \text{ mN}\cdot\text{m}^{-1}$. P(VDF–TrFE) powder from Piezotech Inc. of concentration 0.1 g/l was used. The samples were prepared in Saarbruecken and had structures with 10, 20, 30 and 50 depositions on the glass substrate [4, 5]. For this work we used the samples with 10 and 30 depositions from this series. Film thickness was determined both ellipsometrically [4, 5] and by atomic force microscopy (AFM) technique [6, 11]. For the prepared samples it was determined that one transfer corresponded to one monolayer (ML) with average thickness 0.5 nm [4, 5].

2. Analytical and structural characterization of the films

For structural characterization of the films in this work the atomic-resolution scanning tunnelling microscopy (STM) was used. The obtained images showed that the films could have excellent crystalline structure with the polymer chains parallel to each other in the plan of the film. Besides STM, the structure of LB films was studied by means of X-ray and neutron diffractometry [1–3]. Additionally for characterization of samples atomic force microscopy (AFM), especially piezoelectric force microscopy (PFM) was used for detailed structural characterization of the film surface and width. Both topography and piezoelectric images were performed at the University of Aveiro by PFM method using a commercial Scanning Force Microscope (Multimode, Nanoscope IIIA, Veeco) equipped with a function generator and a lock-in amplifier [6, 11]. No piezoelectric contrast or domains could be found on the piezoelectric image before application of writing voltage, just a weak background signal that could appear due to either self-polarization of the surface layer or to an apparent signal determined by the contact potential difference between the tip and bottom electrode [11].

3. Thermo-stimulated exoelectron emission (TSEE) technique

Thermo-stimulated exoelectron emission (TSEE) was recorded by a photoelectron emission spectrometer for measurements at a vacuum chamber under a pressure of 10^{-4} Pa.

The heating rate of the samples equalled 0.4 grad/s. Necessary addition photostimulation of the second type of sample was provided by ultraviolet (UV) illumination from deuterium source DDS-30. The required photon energy was selected by means of a SF-26 monochromator. The frequency breadth did not exceed 0.08 eV. The values of measured work function Φ were estimated with the uncertainty that did not exceed ± 0.04 eV. For registration of electron emission a very sensitive electron detector was used. The secondary electron multiplier with noise on the level of 0.1–1 electron/second was applied [27].

4. Molecular model and computational approaches

In this work several versions of molecular models for PVDF ferroelectrics were developed and investigated using HyperChem 7.52 as well as 8.0 version (on the base of the various personal computers). For some cases of precise ab initio calculations the Gaussian98 on the Linux cluster of the IMPB RAS was used too. We studied the dependences of the main PVDF electrical properties (dipole momentum, polarization, energies of electron subsystem as well as the total energy of the systems) without and under applied electrical field for the explored molecular models of PVDF ferroelectrics with different length of the molecular chains and various conformations. Various computational methods were used, including quantum-chemical calculations based on the density functional theory (DFT) as well as semi-empirical (PM3) methods, both in restricted Hartree-Fock (RHF) and in unrestricted Hartree-Fock (UHF) approximations. The details of the models and computational approaches are described in the sections given below.

RESULTS AND DISCUSSIONS

1. Thermo-stimulated exoelectron emission (TSEE) data and analysis

The thermo-stimulated exoelectron emission (TSEE) analysis was employed for testing of polarization of the PVDF as well as P(VDF-TrFE) specimens by a the novel non-contacting mode. TSEE analysis is very appropriate for the characterization of surface electronic structure in the produced P(VDF-TrFE) films of the different thickness and compositions. TSEE from dielectric and non metallic materials is typically provided by the thermo-electron emission mechanism [25–27]: the temperature (T) depending processes in the emitter being the modulation factor of the electron emission current (I). In the case of the ferroelectric PVDF (we use further only this abbreviation for short, if not necessary to mark TrFE component) film polarization/depolarization can become a modulation factor. Therefore, the features of the $I(T)$ behavior characterize depolarization of the PVDF film. For the case of our ferroelectric thin films, deposited on a dielectric glass substrate (without any metallic electrodes), distribution of electron energy zones, their tilt and shift in the surface area are schematically presented on fig. 1.

The polarization P in PVDF film and corresponding internal electrical field E_P shifts the electron energy zones, and the thermo-electron work function Φ , as well as electron affinity χ for the case of the plane model of thin PVDF film with thickness x , which are presented on Fig. 1. The resulting change of the electron potential energy $\phi(E_P)$ can be written as the following:

$$\phi(E_P) = -\int_0^{x_0} E_P(P) dx = -E_P \cdot x_0 = -\left(\frac{P}{2\epsilon\epsilon_0}\right) \cdot x_0, \quad (1)$$

where ε is the relative dielectric permittivity and $\varepsilon_0 = 8.8541878... \cdot 10^{-12} \text{ C}/(\text{V}\cdot\text{m})$.

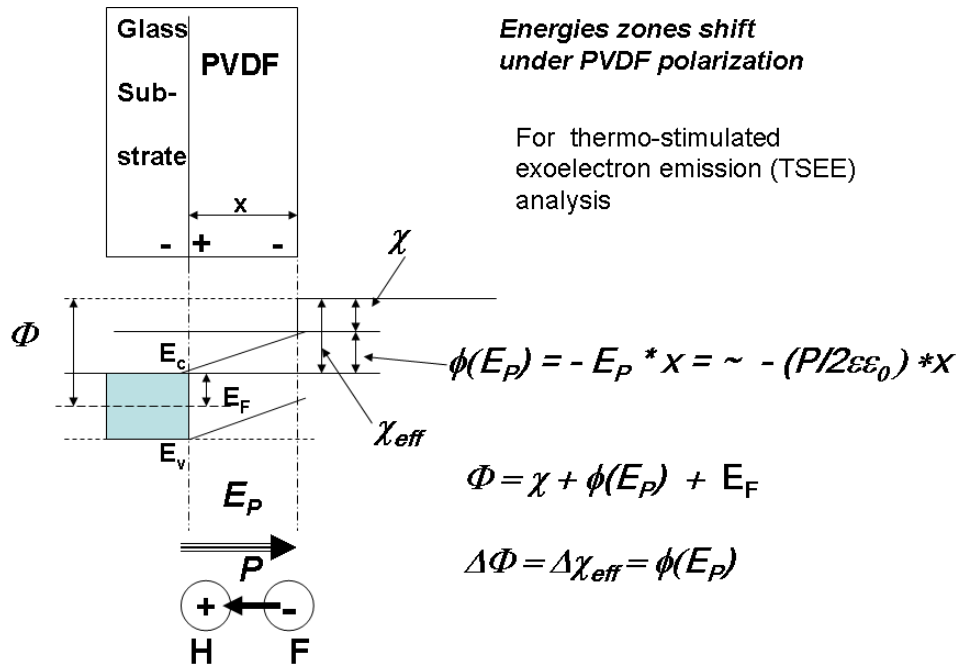


Fig. 1. Schematic of the energy zones and their shift under influence of the polarization electric field of a PVDF (and similar for P(VDF-TrFE)) thin film deposited on a glass substrate: Φ is the thermo-electronic emission work function, χ and χ_{eff} are the affinity and effective affinity of the electron, ϕ is the energy of electric field E_P inside the PVDF (or P(VDF-TrFE)) film with polarization P and thickness x ; E_F is the energy of Fermi level, E_c and E_v are the energies of the conductance and valence bands in the PVDF film.

The TSEE from the PVDF films 10 (10 ML) and 30 (30 ML) monolayers thick (or ~ 5 nm and ~ 15 nm thick, respectively) deposited onto a glass substrate was detected. The TSEE spectra are provided in Fig. 2a. The 30 ML film in contrast with the 10 ML film demonstrates a maximum (at $T_{max} = +100$ °C). So, it means that 10ML film has not any polarization and its reorganization under heating, while 30 ML film has it. Because both PVDF and the glass substrate are insulators, the electrons can escape both from PVDF and the glass local states; there is not enough T to provide thermo-induced emission from the valance band. Taking into account the thermo-electron emission mechanism of TSEE, the maximum obviously can result from the competition between the increased probability of thermo-emission and decreased density of electrons at the local states; both processes are supplied by T . When $T < T_{max}$ the emission of electrons is influenced by the electrical field of polarization (self-polarization). However, at $T > T_{max}$, the thermally induced depolarization “switches off” the electrical field. In this case the thermo-emission electron work function Φ should become smaller. To verify this, the value of Φ has been estimated using the equation of the thermo-emission current:

$$\ln \frac{I}{T^2} = \ln A - \frac{\Phi}{kT}, \quad (2)$$

where A is the emission coefficient, k is the Boltzman constant. The lines (2) for 30 L film are presented in Fig. 2b. The values of Φ calculated from Fig. 2b graph are equal to 1.97 eV at

$T < T_{\max}$ and 0.72 eV, when $T > T_{\max}$. The result (decreasing of Φ after $T > T_{\max}$) is in favor of the above proposed model. Moreover, the temperature induced depolarization corresponds to the changes of the potential $U_P = 1.97 - 0.72 = 1.25$ V or corresponding internal electrical field E_P on the distance equal to 30 ML with $x = 15$ nm: $E_P = 1.25\text{V}/15 \text{ nm} = 0.083 \text{ V/nm} = 8.3 \cdot 10^5 \text{ V/cm} = 0.83 \text{ MV/cm}$; this electrical field results from the PVDF film internal self polarization.

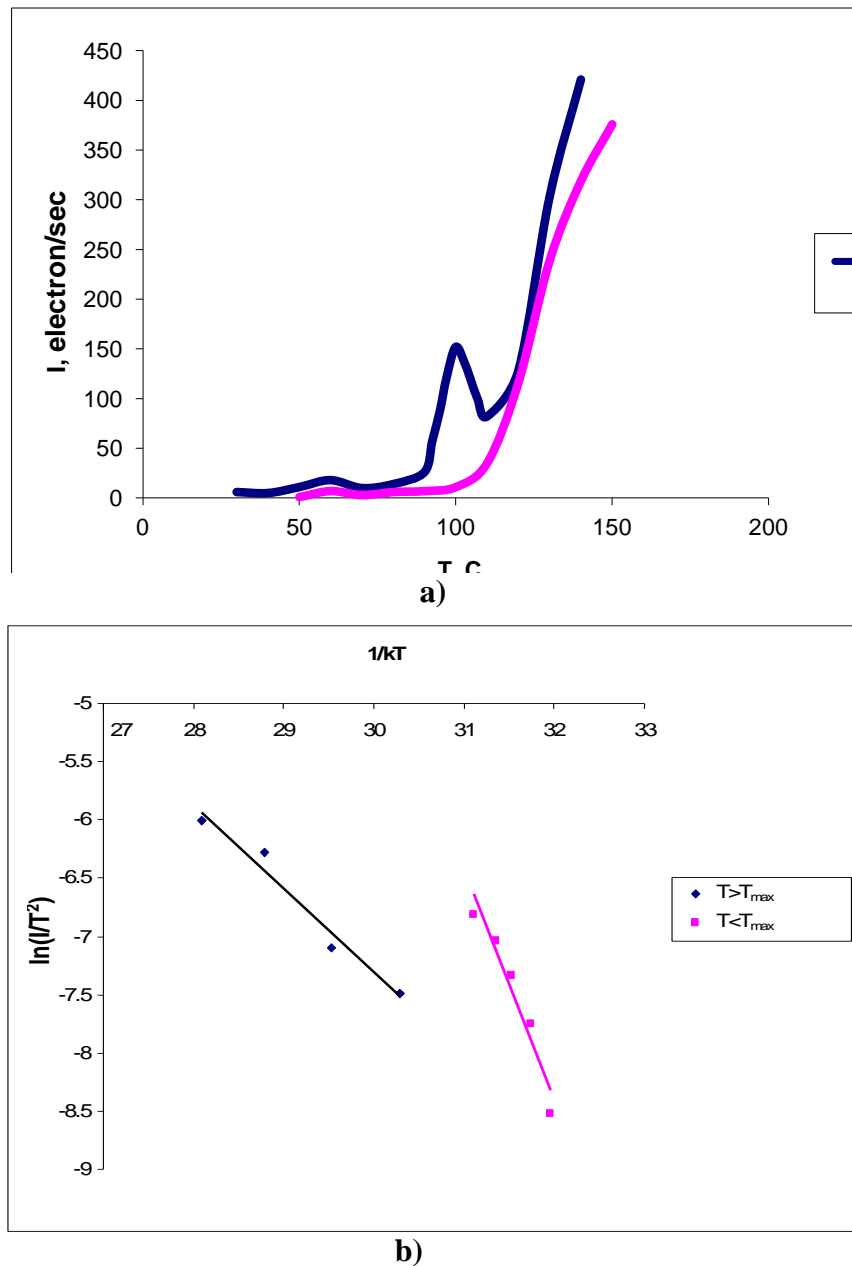


Fig. 2. TSEE spectra of the PVDF films deposited on a glass substrate: a) the PVDF films 10 (10 ML) and 30 (30 ML) monolayers thick; b) the fitted lines of equation (1) for the 30 ML film.

Because the electron potential energy $\phi(E_P)$ is (1), therefore the spontaneous polarization inside this PVDF film can be expressed in absolute value as $P = 2\epsilon\epsilon_0 E_P$. For PVDF films 30 (30 L) monolayers thick ($x \sim 15$ nm) the polarization value, estimated for $\epsilon \sim 10$ (see, for

example, ϵ data from [1,2,28–32] for P(VDF–TrFE)), is equal $P = 0.0147 \text{ C/m}^2 \sim 1.5 \text{ } \mu\text{C/cm}^2$. From [4, 5] data for the similar 30 ML P(VDF–TrFE) (70:30) sample with $d = 16.3 \text{ nm}$ (at $T = 273\text{K}$) polarization is $\sim 5\dots7 \text{ } \mu\text{C/cm}^2$. But this data is obtained directly after polarization in an applied electrical field, while in our case we have data with no electrical field applied (self-polarized) and after long time relaxation. It is known that in similar PVDF films usual relaxation (with time ~ 1 hour) causes drop of polarization value by 40...50 % [3, 4], so it can be lower, $\sim 2\dots3 \text{ } \mu\text{C/cm}^2$. After long storage times it may fall even lower, to $\sim 1 \text{ } \mu\text{C/cm}^2$. It is close to the estimated value in our case.

There was an attempt to polarize the 10ML film too. For this purpose the ultraviolet light radiated the specimen. Alongside its glass substrate was radiated and tested by photoelectron emission analyses to estimate an increment of the induced electrical field, the work function Φ_{pe} being the index of this. The Φ_{pe} was derived using the photoemission current I_{pe} equation

$$I_{pe} = (E_p - \Phi_{pe})^m, \quad (3)$$

where E_p is the energy of the photon, m is the power index.

Radiation increased the value of Φ_{pe} from 5.1 eV to 5.2 eV, that meant that the surface of the glass substrate had been charged negatively (see Fig. 1). After this ultraviolet radiation the TSEE of this PVDF sample demonstrated a maximum at $T_{max} = +120 \text{ C}$ (Fig. 3a). The lines (1) for 10 ML film are presented in Fig. 3b. The values of Φ calculated from Fig 3b graph were equal to 1.34 eV at $T < T_{max}$ and 0.08 eV, when $T > T_{max}$. The result (decreasing of Φ after $T > T_{max}$) is also in favor of the TSEE model given above. Because ultraviolet radiation provides the potential $5.2 - 5.1 = 0.1 \text{ V}$, the native potential by the PVDF film becomes equal to $1.34 - 0.1 = 1.24 \text{ V}$. Therefore the temperature depolarizes the film from 1.24 V to 0.08 V, i.e. to $U_p = 1.16 \text{ V}$, that corresponds to the electrical field E_p of polarization in the film 10 ML thick with $x = 5 \text{ nm}$: $E_p = 1.16 \text{ V}/5 \text{ nm} = 0.232 \text{ V/nm} = 23.2 \cdot 10^5 \text{ V/cm} = 2.32 \text{ MV/cm}$.

As the result, in the PVDF sample with 10 ML, which had not polarization P before the first experiment, after ultraviolet radiation measurements by the TSEE demonstrated polarization in this sample with $E_p \sim 23.2 \cdot 10^5 \text{ V/cm}$.

Comparing this number with the above $8.3 \cdot 10^5 \text{ V/cm}$ characterizing 30 ML self polarized PVDF, one could conclude: 1) the 30 ML PVDF film in contrast with the 10 ML one is self-polarized, 2) the thin (10 ML) PVDF film has a capacity for polarization induced by ultraviolet radiation and can supply polarization 2.8 times as high as that of the 30 ML self polarized film. Corresponding value of polarization of the 10 ML film (for the $\epsilon \sim 10$) is equal to $P \sim 0.0418 \text{ C/m}^2 \sim 4.2 \text{ } \mu\text{C/cm}^2$. This value is close to the measured polarization data for a similar sample $\sim 4\dots6 \text{ } \mu\text{C/cm}^2$ [4, 5]. But it is data without considering relaxation.

It explains why this value for 10 ML is larger than the data for the 30 ML sample, while usually samples with a larger number of ML have greater polarization. The radiation excites electrons to the conductance band both from the glass substrate (the charge of the glass surface had negative potential), and, probably, from the P(VDF–TrFE) valence band too, because for PVDF and P(VDF–TrFE) the energy gap $E_{gap} \sim 5.1\dots5.6 \text{ eV}$ [31–37] is close to the used energy of photons $E_{pe} \sim 5.2 \text{ eV} \dots 5.3 \text{ eV}$. However, the main data on various types of glass demonstrate energy of photons $E_{pe} \sim 6\dots12 \text{ eV}$ [38], only in the case of glass with Fe_2O_3 admixture the energy can be $E_{pe} \sim 5.3\dots5.4 \text{ eV}$. So, these usual values are greater than the values in our experiments. It means that excited electrons come into the conductance bands mainly from the region of the thin PVDF film. Another opportunity connected with the

existence of trap levels close to the bottom of the conductive band (PVDF sample as an n-type semiconductor) is discussed in the section given below.

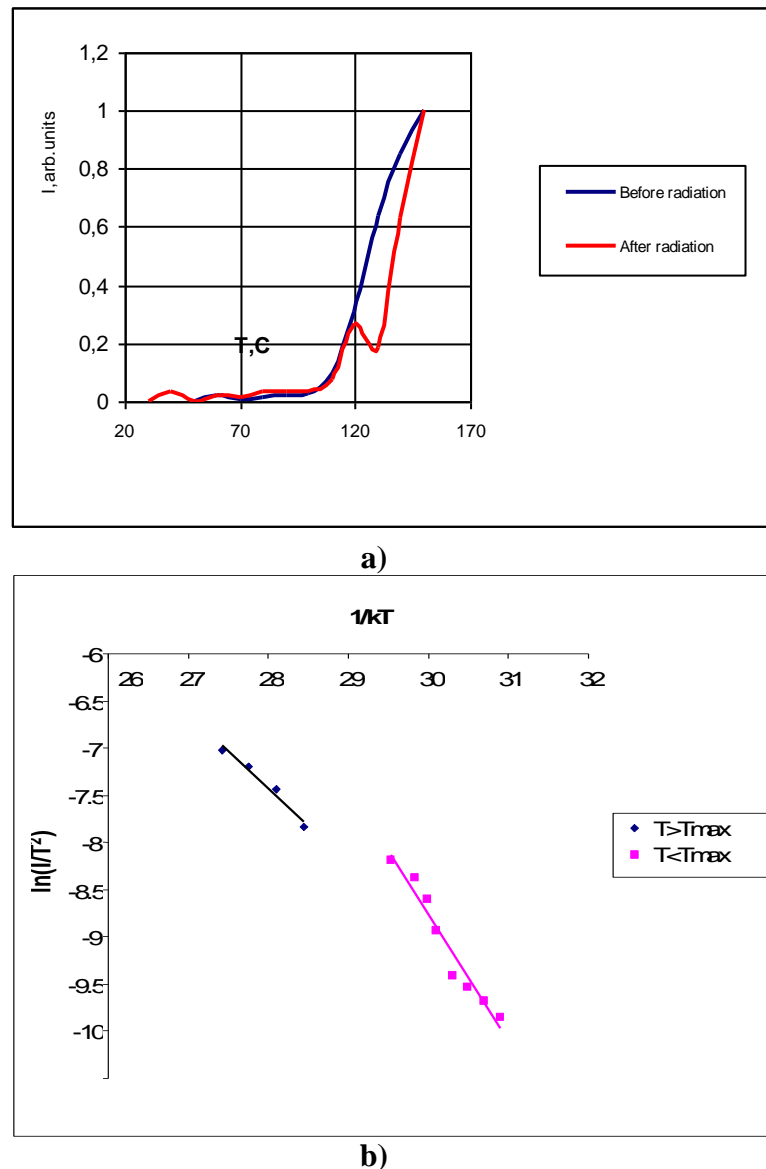


Fig. 3. TSEE spectra of the 10 ML PVDF films deposited on a glass substrate: a) the PVDF films 10 ML thick before and after radiation; b) the fitted lines of equation (1) for the 10 ML film.

On the other hand, it must be emphasized that our direct experiments with pure glass sample show that its surface is charged negatively after this UV illumination. So, excited charges from the glass contribute into joint negative surface charges in any case too. As the PVDF films are very thin and photons can easily pass through them, a considerable part of the contributed charges may arise from the glass. On the negatively charged glass substrate PVDF chains are immediately oriented along arisen from substrate electric field – with positively charged hydrogen atoms towards the glass substrate and negatively charged fluorine atoms outwards the glass. As the result, inside PVDF films stable spontaneous polarization, which can be detected by TSEE spectroscopy method, arises.

2. Molecular modelling and computational analysis

2.1. Analysis of the models of main copolymer units consisting from 2 monomer units

To explain these measured data and for further understanding of the peculiarities of the PVDF copolymer molecular structure in different phase conformations we performed molecular modeling and simulations using HyperChem 7.52 [39] (as well as the new updated version 8.0) with the quantum approach from first principles, namely, density functional theory (DFT) methods, such as the many-parameter exchange-correlation functional method HCTH98, developed by Handy *et al.* [40] and several similar approaches (e.g., Becke-88 functional [41] with Lee–Yang–Parr (LYP) correlation functional [42], in combination with the fastest and most suitable PM3 semi-empirical method [39]. A number of the used DFT functionals both for exchange and correlation have been developed earlier by J.P. Perdew and his collaborators. The Perdew–Wang-91 exchange functional is similar to the Becke-88 functional, but with a somewhat different function [43]. We use it in some cases too for comparison of data. Although DFT is widely used in computational chemistry, the most popular density functional B3LYP has some serious shortcomings, which are being now analyzed and corrected [44]. On the other hand, semi-empirical methods, such as new PM6 methods, are being now developed very fast too [45]. Because of this, it is important for practice to make the most effective combinations of these different approaches.

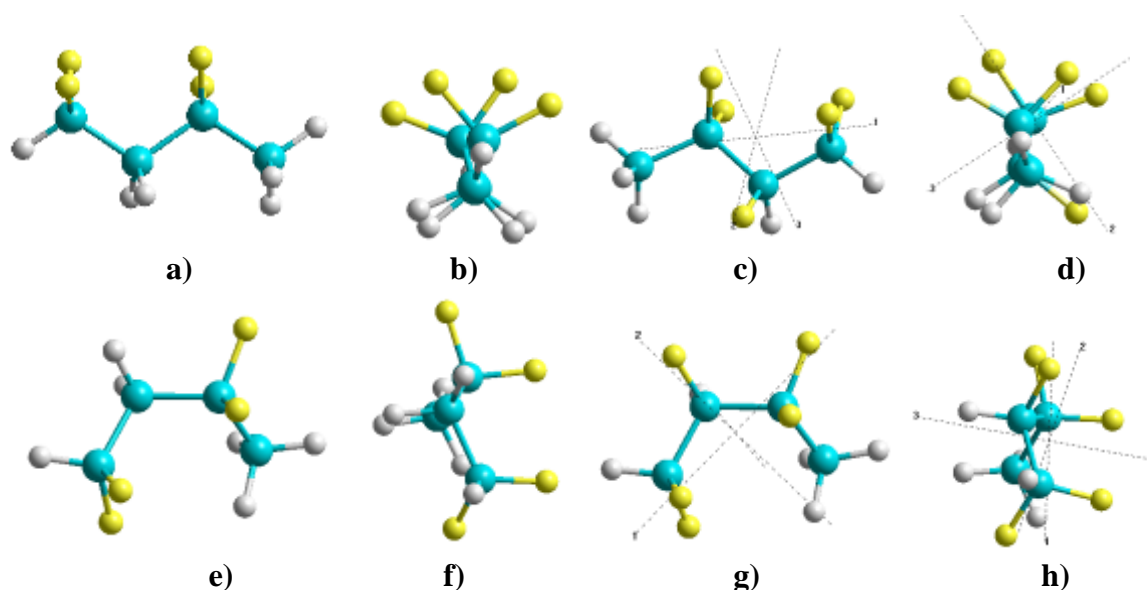


Fig. 4. Structural representation of the modelled polymer building blocks, containing two minimal VDF units ($-\text{CH}_2\text{-CF}_2-$) in the different phase conformations – Trans (T) (upper line) and Gauche (G) (lower line): a) and b) 2VDF-T in Y and Z planes; c) and d) 2(VDF-TrFE)-T in Y and Z planes; e) and f) 2VDF-G in Y and Z planes; g) and h) 2(VDF-TrFE)-G in Y and Z planes.

Firstly we constructed several minimal structural building blocks containing the main PVDF copolymer motive $-\text{CH}_2\text{-CF}_2-$ with TrFE variations and for different conformation phases – Trans (T) and Gauche (G) (fig. 4). The main parameters of these models computed by various methods are presented in table 1. The main obtained values (dipole moments, volume and polarization, E_{HOMO} , E_{LUMO} , E_{gap} , as well as ionization potential I_A and

computed electron affinity EA , corresponding to the measured χ , showed on Fig. 1) are close to calculated by other authors and used in various DFT approaches [32–37]. But most interesting are results connecting the energies of phase transformation and related energies of E LUMO (and EA), which are close to electron affinities.

Table 1. Computed parameters for the different structural conformations with 2 main VDF and VDF-TrFE units (e.i. $P = 2$ for polymers PVDF and P(VDF_TrFE))

Methods	Parameters	PVDF-T	PVDF-G	$\Delta E_{TG} = E_G - E_T$, eV (kcal/mol)	P(VDF-TrFE)-T	P(VDF-TrFE)-G	$\Delta E_{TG} = E_G - E_T$, eV (kcal/mol)
1	2	3	4	5	6	7	8
PM3	E_{tot} , a.u.	-85.602	-85.599	0.0964 (2.622)	-101.2096	-101.2108	-0.033 (-0.76)
	E LUMO, eV	1.4617	1.336	-0.125	0.806	0.717	-0.089
	E HOMO, eV	-12.674	-12.848		-12.73	-12.93	
	E_{gap} , eV	14.136	14.184		13.54	13.64	
	Dipole, D	4.103	2.588		3.235	2.967	
	Volume, A^3	89.58	89.684		92.47	90.78	
	Polarization, C/m^2	0.153	0.096		0.117	0.109	
	EA , eV	1.0945	0.9737	-0.121	0.567	0.312	-0.26
IA , eV	12.500	12.677		12.18	12.97		
DFT 1 (HCT H98)	E_{tot} , a.u.	-555.23	-555.233	-0.077 (-1.77)	-654.4227	-654.42	-0.057 (-1.32)
	E LUMO, eV	1.5129	1.3576	-0.155	0.689	0.854	0.165
	E HOMO, eV	-7.066	-7.324		-7.053	-7.289	
	E_{gap} , eV	8.579	8.681		7.742	8.143	
	Dipole, D	3.592	2.207		2.767	2.514	
	Volume, A^3	89.58	89.68		90.68	90.78	
	Polarization, C/m^2	0.134	0.082		0.102	0.092	
	EA , eV	3.993	3.896	-0.097	3.988	3.699	-0.289
IA , eV	10.16	10.435		9.816	10.381		
DFT 2 (Becke-88, LYP)	E_{tot} , a.u.	-555.27	-555.272	-0.081 (-1.87)	-654.4903	-654.4923	-0.055 (-1.23)
	E LUMO, eV	1.439	1.335	-0.105	0.811	0.976	0.1647
	E HOMO, eV	-6.829	-7.089		-6.81	-7.044	
	E_{gap} , eV	8.506	8.424		7.621	8.019	
	Dipole, D	3.447	2.115		2.647	2.372	
	Volume, A^3	89.58	89.68		90.68	90.78	
	Polarization, C/m^2	0.134	0.082		0.097	0.092	
	EA , eV	3.993	3.896	-0.097	3.988	3.699	-0.289
IA , eV	10.16	10.44		9.816	10.38		

In our case we obtain that the values of the total energy advantage under the phase transition between G and T conformations $\Delta E_{TG} = E_G - E_T$ are following (Table 1):

a) for PVDF it is $\sim 1.8 \dots 1.9$ kcal/mol (or ~ 0.08 eV) for both used DFT methods, in comparison with the value ~ 2.3 kcal/mol in [37]; b) for P(VDF-TrFE) it is ~ 1.3 kcal/mol (~ 0.056 eV) in comparison with ~ 1.46 kcal/mol and ~ 1.92 kcal/mol for two various conformers in [37]. These results prove the truth of the computational description of the direction of phase transitions from T to G in our cases. The PM3 is not as good for the case of pure 2VDF unit (ΔE_{TG} have the opposite sign), but it is appropriate for the 2(VDF-TrFE) case

(with $\Delta E_{TG} \sim 0.8$ kcal/mol). Neither the PM3 gives good results for E_{HOMO} in all cases. But for the energies of the E_{LUMO} and electron affinities EA , especially their changes, the results are very close both for PM3 and for DFT approaches (see Table 1).

Because the electron affinity and corresponding E_{LUMO} energies are most essential for the case of our TSEE method, i.e. thermally excited electrons are emitted from bottom of the conductive band or from E_{LUMO} (see Fig. 1), we are more focused on these points in our further studies.

2.2. Analysis of the influence of the monomer units number on the energie's characteristics of the copolymer chain

We constructed series of models with various lengths and corresponding VDF copolymer units, including TrFE components (for the models we used ratio of concentrations 70:30) for different conformations (T and G). The results of DFT HCTH98 as well as PM3 calculations are shown on Fig. 5 (for E_{HOMO} and E_{gap} data) and on Fig. 6 (for E_{LUMO} data). As it can be seen, the growth of the main polymer units leads to the lowering of all energies, which corresponds to the known data [16, 17]. It is true for both methods having been used (both PM3 and DFT), but while the E_{HOMO} for PM3 manifests half as much energy as by DFT, the E_{LUMO} energies lie in very close areas of values for both methods (Fig. 6). From the obtained E_{LUMO} data we can conclude that for large molecular chains (with numbers of polymer units $\sim 5 \dots 10$) the variations in the energy values between the data by PM3 and DFT methods are not large, despite the very large difference for E_{HOMO} (see Fig. 6 and Fig. 5).

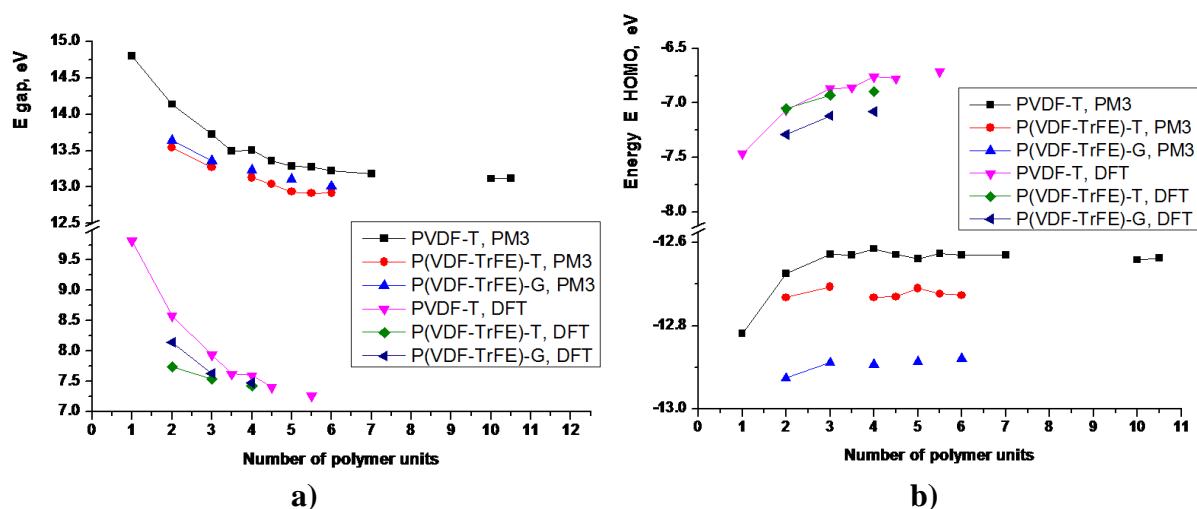


Fig. 5. Relationship between the energies and the number of polymer units: a) the energies of the forbidden zone E_{gap} ; b) the energies of the E_{HOMO} .

At the same time the variations in energies of the E_{LUMO} for various conformations (G and T) increase and reach the value ~ 0.5 eV for large numbers of chain units ~ 10 . Moreover, as one can see for large chains of P(VDF-TrFE)-T this E_{LUMO} value falls to zero and even can be negative for the G conformation of the large P(VDF-TrFE) chain (Fig. 6).

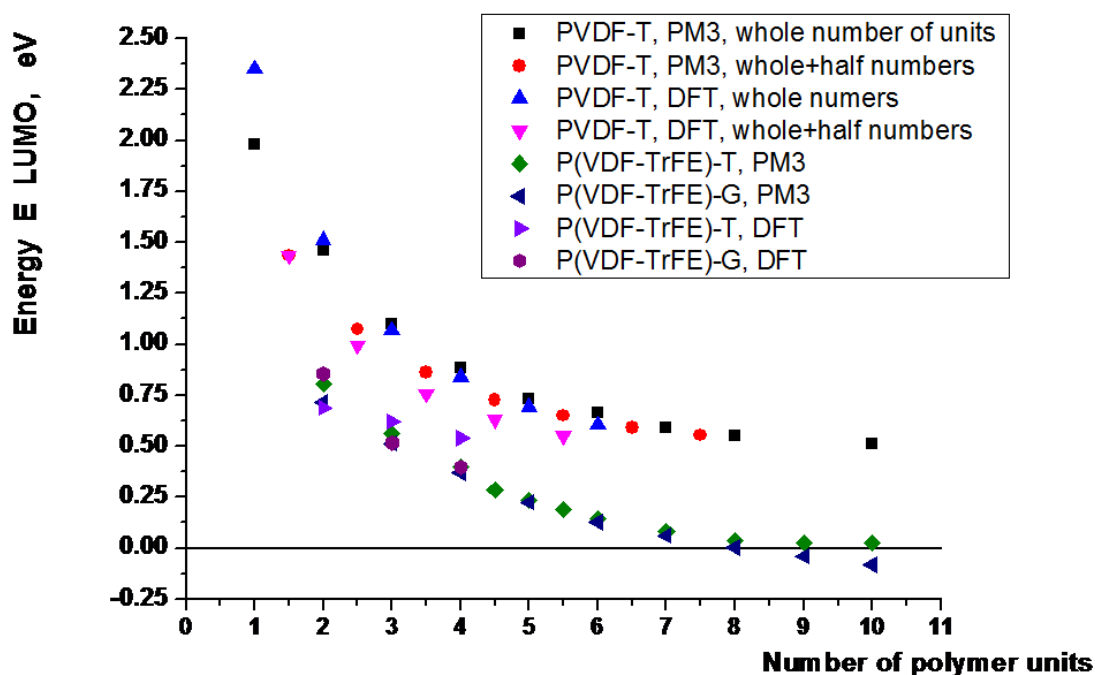


Fig. 6. Relationship between the energies of the $E LUMO$ and the numbers of polymer units for different conformations (T and G) computed by various methods.

So, based on this results we can allow that, unlike pure PVDF chains, mixed P(VDF-TrFE) chains suffer more influence under conditions of the phase transition from T to G through additional thermo-excitation of the electron subsystem, which is connected directly with $E LUMO$ energies, corresponding to the bottom of the conductance band E_c and to the energy of electron affinity (EA , or χ on Fig. 1).

2.3. Model of two interacting long polymer chains

We tried to clarify and test this reasoning by simple models, consisting of two long (10 units) P(VDF-TrFE) chains, which were in parallel or antiparallel dipole orientation in the T conformation and antiparallel in the G conformation (to reach full compensation of total dipole momentum, corresponding to the non-polar paraelectric G phase). The results of the calculations for these models are presented in table 2.

From these data one can see that after the phase transition from T phase to G phase the electron affinity EA is changed from ~ -1.172 eV onto $\sim +0.230$ eV. So, total rise of EA is $\Delta EA \sim 1.40$ eV. It allows electrons to go away from the sample surface easier, as it was in our case after TSEE temperature exposure. The energies of $E LUMO$ in this case are changed from ~ -0.73 eV up to $\sim +0.33$ eV, that is total rise of the $\Delta(E LUMO)$ is ~ 1.06 eV.

Table 2. Data for two P(VDF TrFe) 70:30 chains (10 units) with their various orientations and conformations

Quantity	UHF	PM3 method		
	Spin orb.	2chains 10 un. TRANS Parall	2 chains 10 un. TRANS Oppos	2 chains 10 un. GAUCHE
E_{LUMO} , eV	α	-0.72902	-0.68426	+0.32891
	β	-0.72901	-0.68426	+0.32980
E_{HOMO} , eV	α	-12.2535	-13.3813	-12.6516
	β	-12.2535	-13.3713	-12.6516
E_{LUMO} - $E_{HOMO} = E_g$, eV	$\alpha\alpha$	11.52449	12.69706	12.98055
	$\beta\beta$	11.52450	12.68706	12.98145
$E_{Fermi} = E_g/2$, eV	$\alpha\alpha$	5.762246	6.348529	6.490275
	$\beta\beta$	5.762247	6.343529	6.490724
E_{tot} , a.u.		-1014.025	-1013.993	-1013.959
$E_{binding}$, [kcal/mol]		-12654.90	-12634.97	-12613.25
IE [eV]		12.04264	13.29948	12.53292
		12.04285	13.29971	12.53314
EA [eV]		-1.17175	-0.83292	0.22992
		-1.17176	-0.83295	0.22993
D [D]		32.772	2.444	0.006 ~ 0
D_y (main)		32.772	~ 0	~ 0
Volume, E_i		863.69	860.92	860.01
P [C/m ²]		0.126565	~ 0	~ 0

2.4. Model of double-cell crystal cell of the copolymer

For deeper understanding of this process we developed a model of a crystal cell, which most closely corresponds to the known data [1–7, 11, 16, 17]. The models of the P(VDF-TrFE) double-cell structures both in the Trans (T) and Gauche (G) conformations are presented on fig. 7. We use the usual known data of cell parameters: $a = 0.858$ nm, $b = 0.491$ nm [1 – 6, 16, 17]. The value of E_{LUMO} computed for this model by the PM3 method is ~ -1.568 eV ($E_{HOMO} \sim -10.51$ eV) for the state of the stable Trans (T) conformation.

The calculations for the presented double-cell model in T phase show that the total dipole moment is most preferably oriented in the OY direction (corresponding to the case when it is perpendicular to the surface of the negatively charged glass substrate in the above described experimental sample conditions). The value of the total dipole moment is $D_t \sim D_y \sim 88.4 D$. For the total volume $V_T \sim 1844.42 \text{ \AA}^3$ it corresponds to polarization $P \sim P_y \sim 0.16 \text{ C/m}^2$, which is well comparable with the known data [1–7, 16, 17].

After phase transformation to G phase the dipole moment $D_t \sim D_y \sim 0$ Debye for the total double-cell volume $V_G \sim 1838.17 \text{ \AA}^3$ becomes fully compensated. It leads to zero value of the total polarization $P \sim 0 \text{ C/m}^2$. The values of the electron energies for G conformation are the following: $E_{LUMO} \sim +0.0293$ eV, $E_{HOMO} \sim -9.334$ eV. The schematic of these energy levels is presented on Fig. 8.

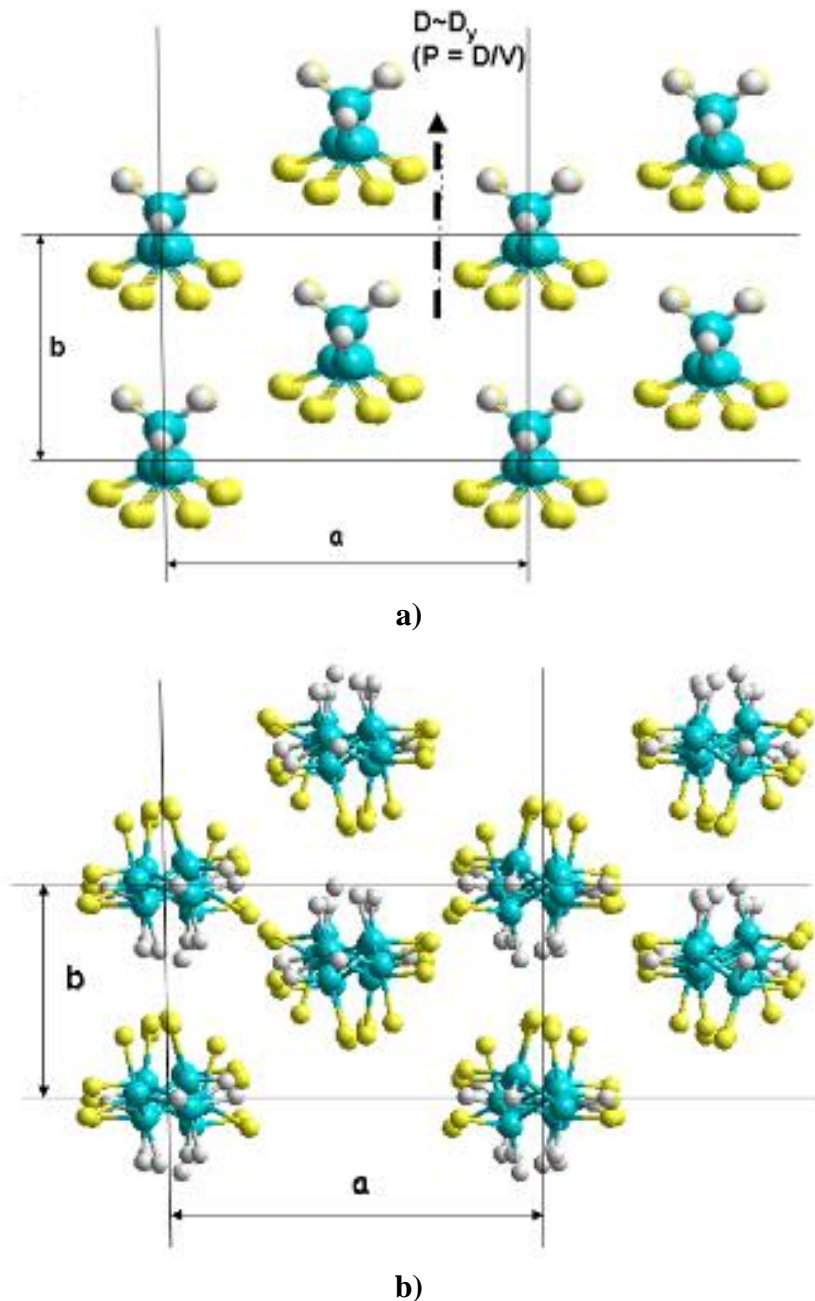


Fig. 7. Model of P(VDF-TrFE) cell in two conformations: a) Trans (T), b) Gauche (G).

So, eventually the E_{LUMO} rises by $\Delta(E_{LUMO}) \sim 1.597$ eV and reaches a close to zero final value of E_{LUMO} , and the same value of the electron affinity. If we compare these data with above TSEE experimental values, we can see that the main order of the values and the tendency of their changes are true (for the 2nd sample we have change of the work function from ~ 1.24 eV to ~ 0.08 eV, and rise of the affinity by ~ 1.16 eV).

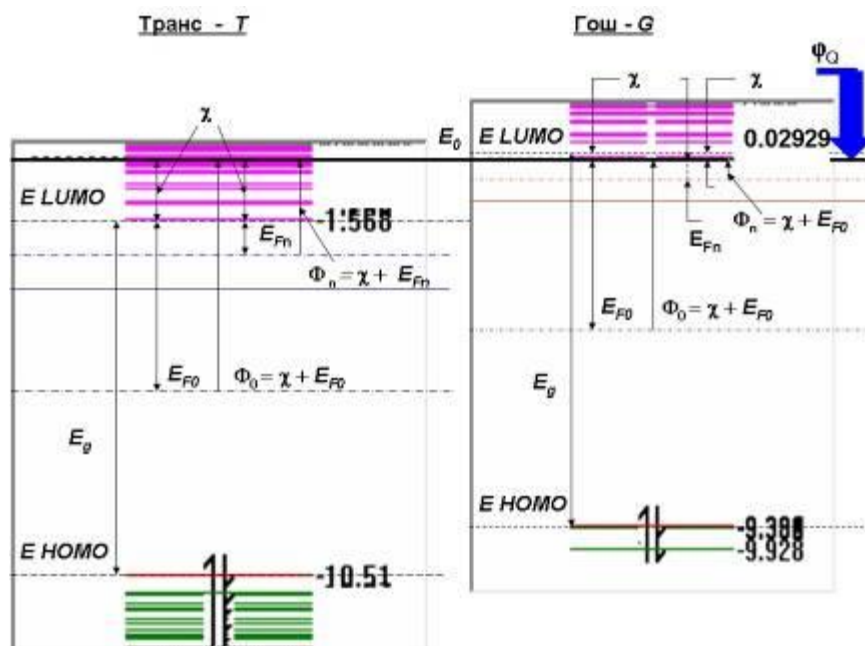
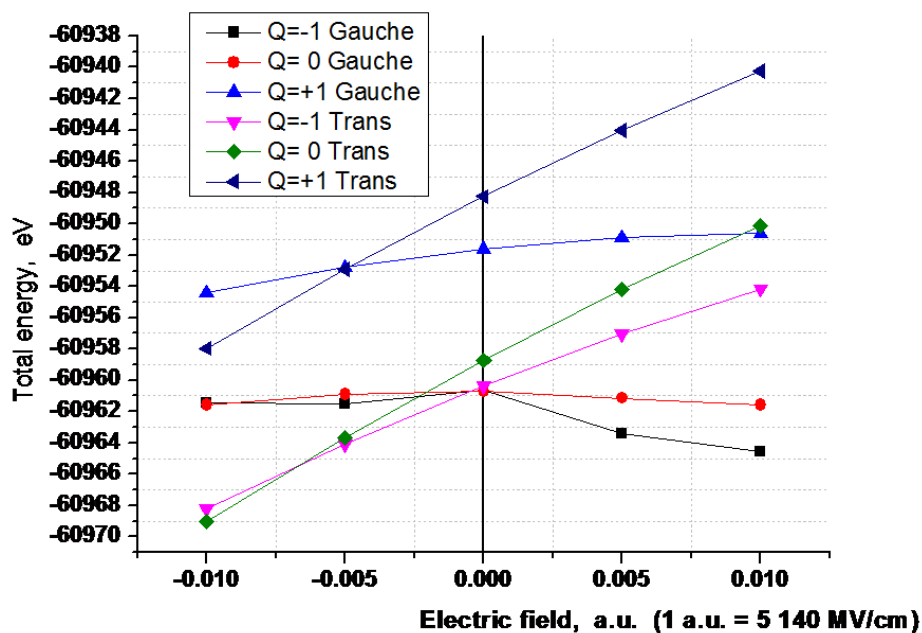


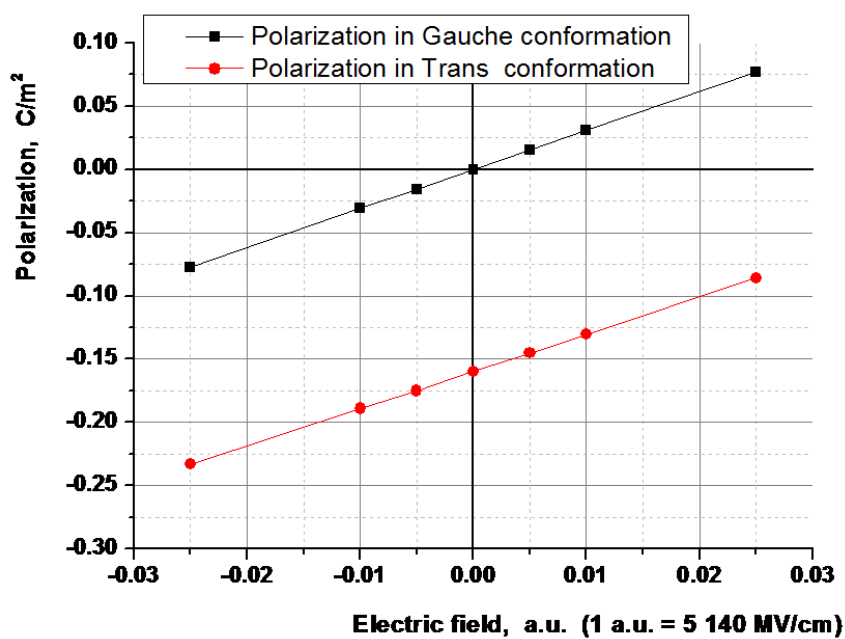
Fig. 8. Schematic of energy zones and their shift under the influence of electric field during phase transition between Trans and Gauche conformations.

3. Main computational results and comparison with experimental TSEE data

Further detailed calculations were made by PM3 method as a faster one comparing with DFT. As it was marked above, while the E_{HOMO} levels and IA energies computed by PM3 differ from DFT and some experimental values, the E_{LUMO} and electron affinities (EA) energies are very close. Because for TSEE the contributions of the thermalized electrons are most essential, these electron energies play the key role in the TSEE processes [26]. Although the E_{HOMO} computed by PM3 lies lower than that computed by DFT, as well as the E_g obtained by PM3 is wider than the one obtained by DFT, nevertheless the behavior and the changes of the energies under phase transition from T to G state of the modeled P(VDF-TrFE) have correct features: the energy of the forbidden zone E_g widens out and all electron energies rise up. The details of the change of the electron bands under electric field from the Trans to Gauche state are presented on the fig. 8: here we calculate also the ionization potential IA corresponding to E_{HOMO} , affinity EA , corresponding to E_{LUMO} , and Fermi energy E_F as half of the forbidden zone E_g , as well as the thermo-electron work function energy as the sum of E_F and EA or/and E_{LUMO} .



a)



b)

Fig. 9. Computed data for double-cell model of P(VDF-TrFE) cluster with the applied electric field changes: a) total energy with different total charges Q for Trans and Gauche conformations; b) polarization for Trans and Gauche conformations.

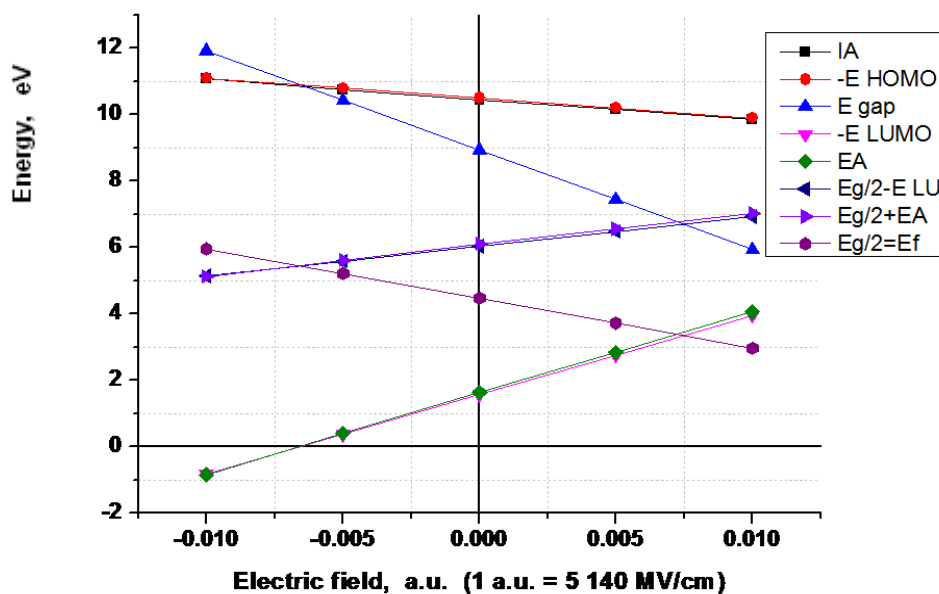
Another important computed data are presented on fig. 9: changes of additional charges ($Q = -1, 0, +1$) allow us to compute the ionization potential IA and affinity EA . Moreover, the computed total energy of system (Fig. 9a) for this molecular cluster (Fig. 7) have the change of the total energy $\Delta E_{T-G} \sim -1.97 \text{ eV} \sim -46.5 \text{ kcal/mol}$. It is equivalent to the total enthalpy changes $\sim 58.18 \text{ J/g}$ for the total molar mass $M_c = 3265.424 \text{ g/mol}$ of the modelled molecular system consisting of 8 molecular chains ($C_{11}F_{14}H_{10}$). Our model of the P(VDF-TrFE)

molecular cluster consists of 280 atoms and corresponds to the real crystal structure of the P(VDF-TrFE) with the content $\sim (70:30)$, in the 2 main conformations – Trans and Gauche.

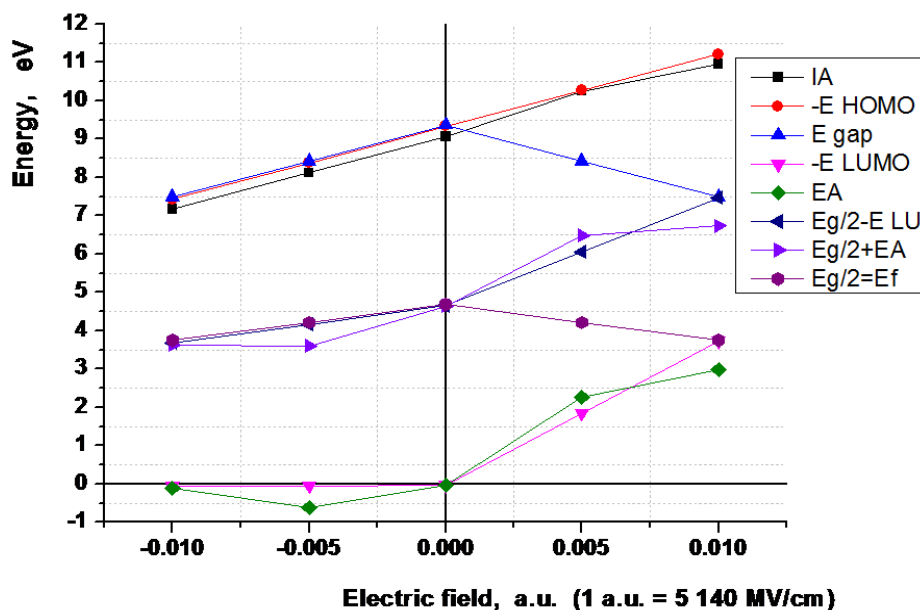
The total energy goes down under transformation from T to G (as it is shown on fig. 9a). This transformation leads to the change of the configuration of each molecular chain and the total volume (volume in Trans state $V_T = 1844.42 \text{ \AA}^3$, while in G state volume $V_G = 1838.17 \text{ \AA}^3$). To be more correct, the comparison must be done for the change of the energy density. We obtain the following calculated data in these cases: $E_{VT} = -33.05034 \text{ eV/\AA}^3$, $E_{VG} = -33.16379 \text{ eV/\AA}^3$, $\Delta E_{V(T-G)} = -0.1135 \text{ eV/\AA}^3$ or it is $\Delta E_{V(T-G)} \sim -2.62 \text{ kcal/mol}$ per volume. These changes correspond to the enthalpy of the process $\Delta H \sim -3.35 \text{ J/g}$ (per volume unit, for the corresponding molar mass $M_c = 3265.424 \text{ g/mol}$ of the modelled molecular cluster). All these obtained data are comparable with all main known published data [37, 46–50] and correspond to these T-G phase transition in the P(VDF-TrFE) (70:30) structures and the crystal cell.

On the other hand, it is known that the P(VDF-TrFE) has n-type semiconducting property with the corresponding energy of the Fermi level E_{Fn} , which differs from E_F in the middle of E_g and is most close to the bottom of the upper conductance band E_c , or the E_{LUMO} energy [3, 5, 51, 52]: $E_{Fn} \sim 0.8 - 0.4 \text{ eV} < E_F \sim 2 - 4 \text{ eV}$ (see fig. 8 and compare with the computed data on Fig. 10), shifted to the bottom of the conductance band (E_c and the corresponding E_{LUMO} energy). In this case, it is evident, that after UV irradiation (with energy of photons $E_{pe} \sim 5.2-5.3 \text{ eV}$ close to the forbidden gap energy $E_g \sim 5.1-5.6 \text{ eV}$ [31–37]) these n-type levels would be excited and become traps for electrons too. The second irradiated P(VDF-TrFE) sample manifests the property of photo-ferroelectrics [53] in this case.

This fact has real evidence here. If we analyze the TSEE spectrum data more thoroughly in comparison with the calculated energy levels (see Figs. 1, 2, 3 and Fig. 8), we can see that for the second sample the energies of the thermo-emission electron work function Φ are shifted on the value of $\phi_Q \sim 0.64 \text{ eV}$ (in comparison with the first non-irradiated sample) both before and after passing through TSEE peak: after T_{max} shift is $\sim 0.72 - 0.08 = 0.64 \text{ eV}$, and before T_{max} the shift is equal to $\sim 1.97 - 1.34 = 0.63 \text{ eV}$, if we neglect the change on the glass surface by 0.1 eV as it was mentioned above. This means that in both cases (before T_{max} – in T state, and after T_{max} – in G state) for the second sample, inside the sample an additional electric field exists (arisen from trapped charges on possible surface levels) and all the energy levels of the system become shifted down in comparison with a “pure” ideal system without these additional levels (see fig. 8). This field corresponds to the following density of the surface charges: $N_Q \sim 7 \cdot 10^{12} \text{ 1/cm}^2$. This is a reasonable value [53]. For illustration of the effectiveness of the proposed molecular modeling approach we present also the density of the E_{HOMO} and E_{LUMO} states for the T model: it shows clearly, that under influence of the internal electrical field (local field [54]), arisen from the existed spontaneous polarization, the electron density distribution (electron clouds) shifts in the direction of the electric field (see Fig. 11).



a)



b)

Figure 10. Computed energy characteristics for the P(VDF-TrFE) model cluster: for Trans conformation, for Gauche conformation. Used abbreviations: IA is the ionization potential, EA is the electron affinity, E_{HOMO} and E_{LUMO} are the highest occupied and low unoccupied molecular orbitals, $E_g = E_{gap} = E_{HOMO} - E_{LUMO}$ is the forbidden energy gap, $E_F = E_g/2$ Fermi level in ideal system, $E_g/2 + EA \sim E_g/2 - E_{LUMO} \sim \Phi$ correspond to the energy level of the thermo-emission electron work function Φ .

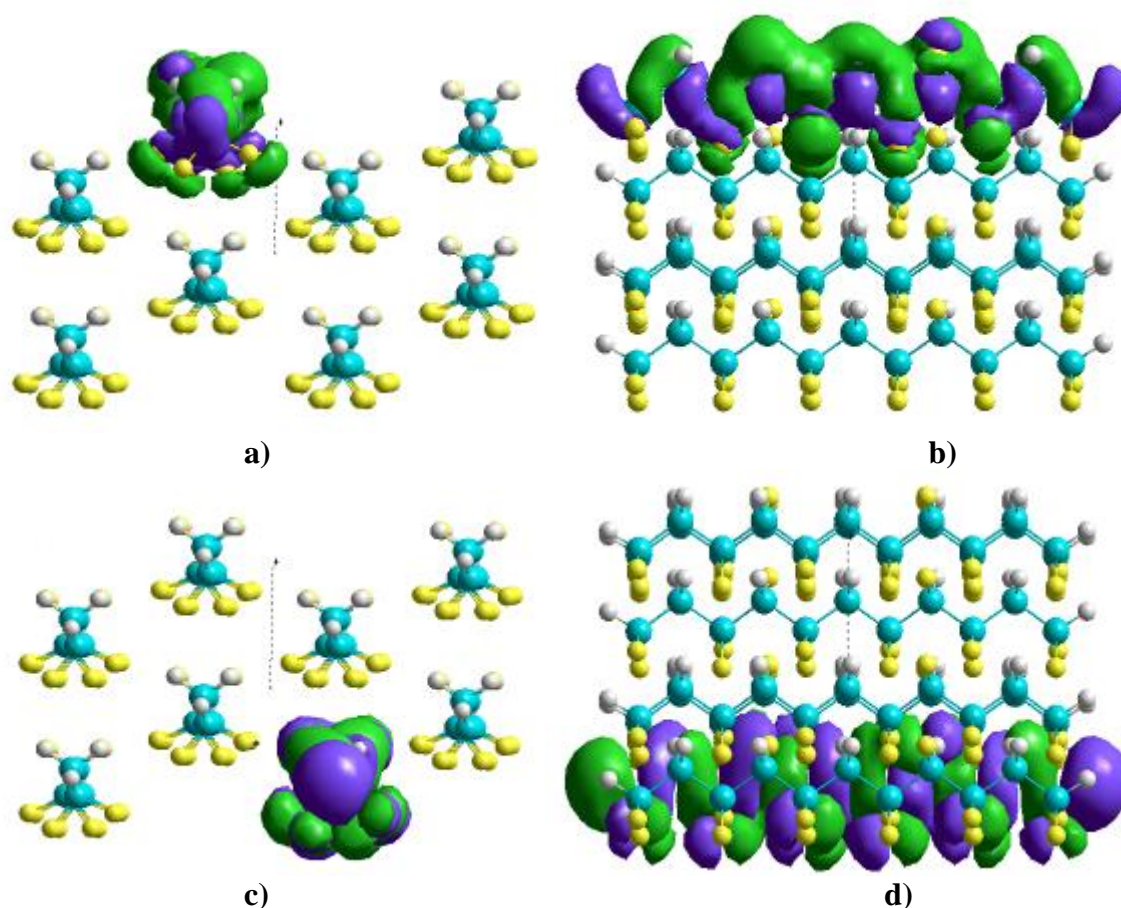


Fig. 11. Images of 3D isosurfaces of electron orbitals for modelled P(VDF-TrFE) 70:30 cell in trans (T) conformation (by HyperChem 8.0): a) and b) LUMO in Z and Y plane orientation; c) and d) HOMO in Z and Y plane orientation.

CONCLUSIONS

The developed new computational molecular models of the PVDF and P(VDF-TrFE) ferroelectric polymers, especially the double-cell cluster model, are very useful for studies of main physical properties of this material at the nanoscale level and give us new data on the energies, both the total energy and for important electronic orbitals. An essential feature of the proposed model is that it can describe phase transformation of these ferroelectric polymers from Trans to Gauche conformations and enables to obtain values of actual changes of the electronic energies and polarization. These data can be compared with experimental data too. But most important is that from this point of view and the constructed model we can find new application of the known thermo-stimulated exoelectron emission technique.

The proposed TSEE technique coupled with the developed molecular modeling approaches allows us to obtain both values of polarization and data on electron affinity and work function of PVDF and P(VDF-TrFE) samples, undergoing phase transition from T to G conformation under temperature heating exposure. The main advantage of this TSEE method is the opportunity of non-contact measurements, which is very important and necessary for some cases. For example, nondestructive control of functioning of a bone's implant, especially with including built-in sensors. Such new smart nanobiotechnology will be very perspective and find wide application in the contemporary nanobiomedicine.

These studies were supported by grants INTAS-05-1000008-8091. V.S.B. is grateful to Fundação para a Ciência e a Tecnologia (FCT, Portugal) for support SFRH/BPD/22230/2005 grant and to DAAD 325-A09/03515/2009 and DFG KL 654/29-1 grants (Germany).

REFERENCES

1. Blinov L., Fridkin V., Palto S., Bune A., Dowben P. and Ducharme S. *Physics-Uspeski*. 2000. V. 43. № 3. P. 243–257.
2. Bune A.V., Fridkin V.M., Ducharme S., Blinov L.M., Palto S.P., Sorokin A.V., Yudin S.G. and Zlatkin A. *Nature (London)*. 1998. V. 391. P. 874.
3. Qu H., Yao W., Zhang J., Dusharme S., Dowben P.A., Sorokin A.V. and Fridkin V.M. *Appl. Phys. Lett.* 2003. V. 82. P. 4322–4324.
4. Kliem H. and Tardos-Morgane R. *J. Phys. D: Appl. Phys.* 2005. V. 38. P. 1860–1868.
5. Tadros-Morgane R. and Kliem H. *J. Phys. D: Appl. Phys.* 2006. V. 39. P. 4872–4877.
6. Gruverman A. and Kholkin A. *Rep. Prog. Phys.* 2006. V. 69. P. 2443–2474.
7. Tolstousov A., Gaynutdinov R., Tadros-Morgane R., Judin S., Tolstikhina A., Kliem H., Ducharme S. and Fridkin V. *Ferroelectrics*. 2007. V. 354. P. 99–105.
8. Li D. and Bonneli D.A. Ferroelectric Lithography. In: *Scanning Probe Microscopy: Electrical and Electromechanical Phenomena at the Nanoscale*. Eds. Kalinin S.V. and Gruverman A. New York: Springer, 2007. P. 906–928.
9. Rodriguez B., Jesse S., Baddorf A. and Kalinin S. *Phys. Rev. Lett.* 2006. V. 96. P. 237602.
10. Rodriguez B.J., Jesse S., Kalinin S., Kim J., Ducharme S. and Fridkin V.M. *Appl. Phys. Lett.* 2007. V. 90. P. 122904.
11. Bystrov V.S., Bdikin I.K., Kiselev D.A., Yudin S.G., Fridkin V.M. and Kholkin A.L. *J. Phys. D: Appl. Phys.* 2007. V. 40. P. 4571–4577.
12. Kang S.J., Bae I., Shin Y.J., Park Y.J., Huh J., Park S.-M., Kim H.-C. and Park C. *NANO Letters*. 2011. V. 11. P. 138–144.
13. Egusa S., Wang Z., Chocat N., Ruff Z.M., Stolyarov A.M., Shemuly D., Sorin F., Rakich P.T., Joannopoulos J.D and Fink Y. *Nature Materials / Advanced online Publication*. 2010. P. 1–6. doi: 10.1038/NMAT2792.
14. Hu Z., Tian M., Nysten B. and Jonas A.M. *Nature Materials*. 2009. V. 8. P. 62–67.
15. Amer S. and Badawy W. *Current Pharmaceutical Biotechnology*. 2005. V. 6. P. 57.
16. Bystrov V.S., Bystrova N.K., Paramonova E.V., Vizdrik G., Saponova A.V., Kuehn M., Kliem H. and Kholkin A.L. *J. Phys: Condens. Matter*. 2007. V. 19. P. 456210.
17. Bystrov V., Bystrova N., Kiselev D., Paramonova E., Kuehn M., Kliem H. and Kholkin A. *Integrated Ferroelectrics*. 2008. V. 99. P. 31–40.
18. Hereida A., Machado M., Bdikin I., Gracio J., Yudin S., Fridkin V.M., Delgadillo I. and Kholkin A.L., *J. Phys. D: Appl. Phys.* 2010. V. 43. № 33. P. 335301.
19. Callegari B. and Belangero W.D. Analysis of the interface formed among the poli(viniilidene) fluoride (piezoelectric and nonpiezoelectric) and the bone tissue of rats. *Acta Ortop.Bras.* 2004. V. 12. № 3. P. 160–166.
20. Mehta R. The hip gets smart. *Materials World Magazine*, 01 Apr 2010. URL: <http://www.iom3.org/news/hip-and-smart-biomaterials> (accessed 17 July 2011).
21. Bystrov V.S., Bystrova N.K., Paramonova E.V. and Dekhtyar Yu.D. Interaction of charged hydroxyapatite and living cells. I. Hydroxyapatite polarization properties. *Mathematical biology and bioinformatics*. 2009. V. 4. № 2. P. 7–11. URL: [http://www.matbio.org/downloads_en/Bystrov_en2009\(4_7\).pdf](http://www.matbio.org/downloads_en/Bystrov_en2009(4_7).pdf) (accessed 17 July 2011).

22. PERCERAMICS. URL: <http://www.perceramics.vip.lv/> (accessed 17 July 2011).
23. Dekhtyar Yu., Bystrov V., Khlusov I., Polyaka N., Sammons R. and Tyulkin F. Hydroxyapatite Surface Nanoscaled characterization and Electrical Potential Functionalization to Engineer Osteoblasts Attachment and Generate Bone Tissue. In: *The Society For Biomaterials 2011 Annual Meeting & Exposition* (April 13–16, 2011, Orlando, Florida, USA). A 519.
24. Lines M.E. and Glass A.M. *Principles and Applications of Ferroelectrics and Related Materials*. Clarendon Press: Oxford, 1979.
25. Minc R.I., Mil'man I.I. and Kryuk V.I. *Physics-Uspekhi* (Russian). 1976. V. 19. № 8. P. 697–707.
26. Dekhtyar Yu.D. and Vinyarskaya Yu.A. Exoelectron analysis of amorphous silicon. *J. Appl. Phys.* 1994. V. 75. № 8. P. 4201–4207.
27. Dekhtyar Yu.D. Photo-, dual- and exoelectron spectroscopy to characterize nanostructures. In: *Functionalized Nanoscale Materials, Devices and Systems NATO Science for Peace and Security Series B: Physics and Biophysics*. Eds. Vaseashta A. and Mihailescu I.N. Springer Science + Business Media B.V. 2008. P. 169–183.
28. Marcus M.A. *Ferroelectrics*. 1982. V. 40. P. 29–41.
29. Furukawa T. *Ferroelectrics*. 1984. V. 57. P. 63–72.
30. Kimura K. and Ohigashi H. *Jpn. J. Appl. Phys.* 1986. V. 25. P. 383.
31. Newnham R.E., Sundar V., Yumnirun R., Su J. and Zhang Q.M. *J. Phys. Chem. B*. 1997. V. 101. P. 10141–10150.
32. Xiao J., Zhou X., Zhang Q.M. and Dowben P.A. *J. Appl. Phys.* 2009. V. 106. P. 044105.
33. Choi J., Dowben P.A., Pebley S., Bune A.V. and Ducharme S. *Phys. Rev. Lett.* 1998. V. 80. № 6. P. 1328–1331.
34. Elashmawi I.S. and Hakeem N.A. *Polymer Engineering and Science*. 2008. V. 48. № 5. P. 895–901.
35. Elashmawi I.S., Abdelrazek E.M., Ragab H.M. and Hakeem N.A. *Physica B*. 2010. V. 405. P. 94–98.
36. Mandal D., Henkel K., Muller K. and Schmeiber D. *Bull. Mater. Sci.* 2010. V. 33. № 4. P. 457–461.
37. Ortiz E., Cuan A., Badillo C., Cortes-Romero C.M., Wang Q. and Norena L. *Int. J. Quantum Chem.* 2010. V. 110. P. 2411–2417.
38. Arbuzov V.I. *Fundamentals of radiation optic materials*. St-Peterburg, 2008. 284 p. (in Russ.).
39. Hypercube 2002 *HyperChem. Tools for Molecular Modeling*. URL: <http://www.hyper.com/?tabid=360> (accessed 17 July 2011).
40. Hamprecht F.A., Cohen A.J., Tozer D.J., and Handy N.C. *J. Chem. Phys.* 1998. V. 109. P. 6264–6271.
41. Becke A.D. *Phys Rev A*. 1988. V. 38. P. 3098–3100.
42. Johnson B.G., Gill P.M. and Pople J.A. *J. Chem. Phys.* 1993. V. 98. P. 5612–5626.
43. Perdew J.P., Chevary J.A., Volsko S.H. Jackson K.A., Pederson M.R., Singh D.J., and Fiolhais C. *Phys. Rev. B*. 1992. V. 46. P. 6671–6687.
44. Zhao Y. and Truhlar D.G. *Accounts of Chemical Research*. 2007. V. 41. № 2. P. 157–167.
45. Stewart J.J.P. *J. Mol. Model.* 2008. V. 14. P. 499–535.
46. Su H., Strachan A. and Goddard W.A.III. *Phys. Rev. B*. 2004. V. 70. P. 064101.

47. Guo S.S., Sun X.H., Wang S.X., Xu S., Zhao X.-Z. and Chan H.L.W. Thermal and structural properties of high-energy electron irradiated Poly(Vinylidene Fluoride-Trifluoroethylene) copolymer blends. *Mater. Chem. and Phys.* 2005. V. 91. P. 348–354.
48. Guo S.S., Sun C.L., Wu T.S., Zhao X.Z. and Chan H.L.W. Thermal study on structural changes and phase transition in high-energy electron-irradiated blends of P(VDF–TrFE) copolymers. *J. Mater. Sci.* 2007. V. 42. P. 1184–1189.
49. Li W., Meng Q., Zheng Y. Zhang Z., Xia W., and Xu Z. *Appl. Phys. Lett.* 2010. V. 96. P. 192905.
50. Gregorio R.Jr. and Botta M.M. *J Polymer Sci: Part B: Polymer Physics.* 1998. V. 36. P. 403–414.
51. Duan C-G., Mei W.N., Harfy J.R., Ducharme S., Choi J. and Dowben P.A. *Europhys. Lett.* 2003. V. 61. № 1. P. 81–87.
52. Dowben P.A., Xiao J., Xu B., Sokolov A. and Doudin B. *Applied Surface Sciences.* 2008. V. 254. № 14. P. 4238–4244.
53. Fridkin V.M. *Photoferroelectrics.* Springer-Verlag: NY- Berlin, 1979.
54. Kliem H. *Advances in Solid State Physics.* 2003. V. 43. P. 861–874.

Received December 21, 2011.

Published January 19, 2012.